

Characterization of *anillin* mutants reveals essential roles in septin localization and plasma membrane integrity

Christine M. Field^{1,†}, Margaret Coughlin¹, Steve Doberstein², Thomas Marty^{3,*} and William Sullivan⁴

¹Department of Systems Biology, Harvard Medical School, Boston MA 02115, USA

²Five Prime Therapeutics, South San Francisco CA 94080, USA

³Howard Hughes Medical Institute, Developmental Genetics Program, Skirball Institute and Department of Cell Biology, New York University School of Medicine, New York, NY 10016, USA

⁴Department of Molecular, Cell and Developmental Biology, Sinsheimer Laboratory, University of Santa Cruz, Santa Cruz, CA 95064, USA

*Present address: Swiss Parliamentary Services, Federal Parliament Building, 3003 Bern, Switzerland

†Author for correspondence (e-mail: cfield@hms.harvard.edu)

Accepted 1 April 2005

Development 132, 2849-2860

Published by The Company of Biologists 2005

doi:10.1242/dev.01843

Summary

Anillin is a conserved component of the contractile ring that is essential for cytokinesis, and physically interacts with three conserved cleavage furrow proteins, F-actin, myosin II and septins in biochemical assays. We demonstrate that the *Drosophila scraps* gene, identified as a gene involved in cellularization, encodes Anillin. We characterize defects in cellularization, pole cell formation and cytokinesis in a series of maternal effect and zygotic *anillin* alleles. Mutations that result in amino acid changes in the C-terminal PH domain of Anillin cause defects in septin recruitment to the furrow canal and contractile ring. These mutations also strongly perturb cellularization, altering the timing and rate of furrow ingression. They

cause dramatic vesiculation of new plasma membranes, and destabilize the stalk of cytoplasm that normally connects gastrulating cells to the yolk mass. A mutation closer to the N terminus blocks separation of pole cells with less effect on cellularization, highlighting mechanistic differences between contractile processes. Cumulatively, our data point to an important role for Anillin in scaffolding cleavage furrow components, directly stabilizing intracellular bridges, and indirectly stabilizing newly deposited plasma membrane during cellularization.

Key words: Cellularization, cytokinesis, Anillin, septin, PH domain, *Drosophila*

Introduction

Cytokinesis in animal cells occurs by ingression of a cleavage furrow, driven by constriction of an actomyosin-based contractile ring coupled to insertion of new plasma membrane. An important unanswered question is how are furrow ingression and new membrane deposition coordinated (Finger and White, 2002; O'Halloran, 2000)? The *Drosophila* embryo provides an interesting model system with which to address this question and the general cell biology of furrowing. During the syncytial blastoderm stage, typical cytokinesis does not occur, but transient furrows ingress to keep mitotic spindles separate. At this stage, pole cells separate from the yolk mass by a type of cytokinesis that has been little studied. Later, during a process called cellularization, interconnected furrows ingress between each nucleus and synchronously partition the embryo into ~6000 individual cells (Foe et al., 1993). After cellularization, conventional cytokinesis starts in the mitotic domains of the gastrulating embryo (Foe, 1989).

Cellularization is more complex than conventional cytokinesis. It requires an estimated 25-fold increase in surface area during a single cell cycle (Lecuit and Wieschaus, 2000), and is thus useful for exploring the coupling between actomyosin contraction and insertion of new plasma

membrane. It also requires ingression in two different planes. Initially, furrows ingress perpendicularly to the embryo surface. The tips of cellularization furrows are called furrow canals, and they interconnect as an almost hexagonal network surrounding each nucleus. Ingression of the plasma membrane occurs in at least two stages that differ in rate (initially slow, then fast) and mechanism, with certain mutations selectively affecting one stage (Schejter and Wieschaus, 1993). Later, once the furrow canals pass the nuclei, ingression also occurs parallel to the embryo surface. The furrow canals broaden and become almost triangular-shaped in cross-section, and the network transforms into an almost hexagonal array of contractile rings. These constrict around the base of each nucleus, individualizing the cells. Constriction is incomplete. The newly formed cells remain connected to the yolk mass by a thin neck of cytoplasm or 'stalk' as the embryo initiates gastrulation movements (Rickoll, 1976).

Given their rich contractile biology, *Drosophila* embryos have been useful for investigating the mechanism of furrowing. As expected, embryonic furrows contain the contractile proteins F-actin (Warn and Robert-Nicoud, 1990) and cytoplasmic Myosin II (Young et al., 1991; Royou et al., 2004). They also contain septins and Anillin, conserved furrow components whose function is less clear. Septins were

discovered as CDC mutants in budding yeast and were implicated in animal cytokinesis by analysis of mutations in the *Drosophila* septin Peanut (reviewed by Field and Kellogg, 1999; Trimble, 1999; Mitchison and Field, 2002). Peanut was later shown to be involved in cellularization (Adam et al., 2000). Biochemical investigation in *Drosophila* embryos showed that septins bind GTP and assemble into heteromeric complexes and filaments (Field et al., 1996). Their molecular function is unknown, although septins have been implicated in vesicle trafficking (Beites et al., 1999).

Anillin was originally isolated from *Drosophila* embryos by affinity chromatography on F-actin (Field and Alberts, 1995) and homologs were later found in vertebrates (Oegema et al., 2000; Straight et al., 2005) and *C. elegans* (see Maddox et al., 2005). Anillin is required for cytokinesis in *Drosophila* and vertebrate tissue culture cells (Oegema et al., 2000; Somma et al., 2002; Kiger et al., 2003; Rogers et al., 2003; Echard et al., 2004; Straight et al., 2005), but its function during furrowing remains unclear. Mid1 and Mid2, two proteins with more limited homology to Anillin, play central roles in cytokinesis in *S. pombe* (Berlin et al., 2003; Paoletti and Chang, 2000; Tasto et al., 2003).

Anillin is a multi-domain protein that physically interacts with several other cleavage furrow components in vitro. Its N terminus contains a region that binds and bundles F-actin (Field and Alberts, 1995; Oegema et al., 2000), and a second region that binds phosphorylated cytoplasmic Myosin II (Straight et al., 2005). Its C-terminus comprises a predicted PH domain, an ~100 amino acid module often implicated in binding to membranes via inositol lipids (Lemmon, 2004; Lemmon et al., 2002). The C-terminal region of vertebrate Anillin was implicated in septin binding by expression of truncated protein and biochemical assays (Oegema et al., 2000; Kinoshita et al., 2002), but the physiological relevance of that proposed interaction was not tested. To explore the function of Anillin, in particular its potential role in coupling cytoskeletal and membrane dynamics, we analyzed the effects of a series of mutations in Anillin on the diverse, cell cycle regulated furrows in the early *Drosophila* embryo.

Materials and methods

Genetics

All crosses were carried out at 25°C under standard conditions.

In rescue experiments, full-length anillin cDNA was inserted into the Germ9 P-element transformation vector (Serano et al., 1994) and injected into 1-hour-old *Drosophila* embryos.

Eggs were collected from homozygous *anillin*^{RV/RV} females carrying the wild-type transgene, and the percentage that hatched was scored. For complementation tests (see Table S1 in the supplementary material), *scraps/anillin* alleles were maintained over a balancer chromosome containing *Cy*. In all tests, the ratio of homozygous *scraps* adults to the total number of viable adults (*anillin* homozygotes plus *anillin/Cy* heterozygotes) was scored. If the *anillin* mutation does not affect adult viability, the expected ratio would be 1/3 (33%) (see Table S1, column 2 in the supplementary material). When examining maternal/zygotic combinations, *anillin*^{maternal}/*Cy* flies were crossed with *anillin*^{zygotic}/*Cy* and adult viability scored as above. The strong *anillin* maternal alleles could not rescue the lesions caused by the Heitzler zygotic alleles or deficiencies (Schupach and Wieschaus, 1989), indicating that the *anillin* gene probably has the same function both maternally and zygotically. For the maternal genes, combinations of alleles were mated, adult survival scored and then egg hatchability was examined.

Sequencing of *scraps* alleles

Sequencing was carried out at the Biopolymers Facility at Harvard Medical School (HMS) (<http://genome.med.harvard.edu>) and the HHMI sequencing facility at Rockefeller University. At HMS, the entire anillin genomic region for alleles HP and RS was sequenced. In addition, the 3' end (corresponding to the C-terminal 266 amino acids) was sequenced in the genotypes PQ/RS, HP/Cy, RS/Cy, RV/Cy and RV/RV. To generate sequencing templates, a series of overlapping PCR products of 1-1.5 kb in length were produced using Turbo Pfu polymerase. At the HHMI facility, sequencing templates encompassing the full-length gene were generated by PCR of the genomic region of *anillin*^{B26-35}, *anillin*^{C82-45} and *anillin*^{PE}/*anillin*^S using a Long-Range High Fidelity PCR kit (Roche). In addition to the wild-type *anillin* sequence in FlyBase, sequences were compared with a full-length *anillin* genomic sequence from the stock P3427, generated during the cloning of the *blownfuse* gene (Doberstein et al., 1997).

Immunofluorescence

Three different fixations were used for embryos. The fixative for F-actin was 18.5% formaldehyde in PBS/heptane (1:1). Embryos were gently swirled for 20 minutes and then hand devitellinized with a tungsten needle. For Peanut, the fixative was cold methanol/heptane (1:1) for 30 seconds, followed by methanol popping. For Myosin II and Neurotactin a combination of heat treatment and methanol fixation was performed (Peifer et al., 1994). Imaginal discs were dissected from 3rd instar larvae into PBS and immediately fixed in 10% formaldehyde in PBS with 5 mM EDTA, swirling slowly for 20 minutes. Topro Dye, T-3605 (Molecular Probes) was used to stain DNA in imaginal discs. Anti-Anillin (Field and Alberts, 1995), anti-Peanut (Field et al., 1996) and anti-Myosin II (Foe et al., 2000) were all used at 1 µg/ml. Anti-Neurotactin (Developmental Studies Hybridoma Bank, University of Iowa) was used at 1/200. F-actin was stained with Rhodamine-phalloidin (Sigma).

Imaging

For immunofluorescence, samples were imaged on a Nikon TE2000 inverted microscope with a PerkinElmer Spinning Disk confocal (Nikon Imaging Facility at Harvard Medical School). For DIC imaging of cellularization, the chorion was removed by hand, embryos covered with Halocarbon oil, Series 700 (Halocarbon Products, Hackensack, NJ) and filmed (the center of the dorsal embryo surface) at 22°C using a Nikon TE3000 inverted microscope with a 60× water immersion lens. Kymographs were generated using Metamorph software (Universal Imaging). For each genotype, four to eight embryos were filmed and ingress rates measured. Of these, two or three embryos/genotype were kymographed.

Western blots

Blots were carried out using standard conditions. Zero- to 2-hour-old embryos were homogenized in 2× PAGE sample buffer, boiled for 2 minutes and then diluted 1:1 with 8 M urea. Actin is probed with a monoclonal antibody from ICN.

Transmission electron microscopy

Staged embryos were dechorinated for 1.5-2.0 minutes in 50% bleach, fixed, thin sectioned (~65-70 nm sections) and stained with uranyl acetate and lead citrate using a previously described method (Rickoll, 1976). Fresh acrolein was used in each fixation and each fixation included one or more wild-type embryos as controls. Sections were examined on a JOEL 12000. For the majority of embryos, thick sections (~1 µm) were also generated and stained for light microscopy with 1% Toluidine Blue. These were examined to determine developmental stage and confirm that the phenotypes observed were representative.

Results

The *anillin* gene is mutated in *scraps* alleles

To find mutations in Anillin, we sought P-element insertions near its map location, 43DE (Field and Alberts, 1995). We sequenced the genomic region around the insertion site in line P3427, revealing a P-element insertion 53 bp upstream of a potential *anillin* start codon. The *scraps* gene also maps in this region. A screen for recessive female sterile mutations (Schupbach and Wieschaus, 1989) isolated six maternal effect alleles in this gene, designated *scraps*^{RS}, *scraps*^{PQ}, *scraps*^{HP}, *scraps*^{PE}, *scraps*^{RV} and *scraps*^{PB}. Females homozygous for any of these alleles, or trans-heterozygous for any allelic combination, lay morphologically normal eggs that fail to hatch. Observation of mutant embryos using bright-field microscopy showed cellularization defects. Complementation tests over a deficiency of the region revealed a zygotic function for *scraps* (Schupbach and Wieschaus, 1989) and a later study identified two zygotic alleles, *scraps*⁷ and *scraps*⁸ (Heitzler et al., 1993). Two additional maternal effect alleles, *scraps*^{B26-35} and *scraps*^{C82-45}, have recently been identified (T.M. and R. Lehmann, unpublished). In complementation tests, we found that the P3427 insertion line is allelic to *scraps* (see Table S1 in the supplementary material).

To confirm that Anillin is the product of the *scraps* gene, we performed rescue experiments by injecting anillin cDNA. All the embryos from *scraps*^{RV/RV} mothers that received the transgene were rescued to hatching, and ~90% of these developed into fertile adults (data not shown). We conclude that Anillin is essential for embryonic viability and is the product of the *scraps* gene. We propose renaming the gene *anillin* and maintaining the same allelic superscripts, and will follow this convention for the remainder of the manuscript.

Changes in conserved amino acids in the Anillin PH domain result in strong maternal effect alleles

We next ordered the *anillin* mutations into an allelic series, scoring adult viability in complementation tests between maternal and zygotic alleles (Fig. 1A; see Table S1 in the supplementary material). Three maternal alleles (*anillin*^{HP}, *anillin*^{RS} and *anillin*^{PQ}) were lethal in combination with the zygotic alleles *anillin*^{7,8} (Table S1) and with a deficiency of the region (Schupbach and Wieschaus, 1989). We will refer to these as strong maternal alleles. Other maternal effect alleles allowed development to adulthood when tested over either a deficiency of the region (*anillin*^{PE} and *anillin*^{RV}) (Schupbach and Wieschaus, 1989) or the zygotic allele *anillin*⁸ (*anillin*^{B26-35} and *anillin*^{C82-45}) (data not shown). We refer to these as weak maternal alleles, although one of them had a strong defect in pole cell formation, discussed below.

To identify the location of the genetic lesions, the entire genomic region containing *anillin* was sequenced in five maternal alleles. Two additional maternal alleles were sequenced at their C terminus only (see Table S2 in the supplementary material). Mutations were found in *anillin* exons in every case. The three strong maternal alleles contained mis-sense mutations resulting in changes in conserved amino acids at the N-terminal region of the PH domain (Fig. 1B,C). An additional amino acid change (V1055S) was present at the junction between the PH domain and the rest of the protein in all five of the Schupbach/Wieschaus alleles examined (both weak and strong). The possible contribution to the phenotype of this additional mutation was not separately evaluated. Western blotting revealed that the quantity of Anillin protein and its migration on SDS-PAGE was similar in extracts of wild type and all of the maternal alleles tested. (Fig. 1D). We conclude that the amino acid

Fig. 1. Genetic, sequence and western blot analysis of *scraps* (*anillin*) alleles. (A) An allelic series of *scraps* alleles from complementation data in Table S1. Genes with a stronger phenotype are on the right. (B) Schematic of Anillin domain structure; MY, Myosin II-binding region; ACT, F-actin binding region; AH, Anillin homology region; PH, pleckstrin homology domain, and (Septin binding) the region required for Anillin recruitment of septins to F-actin bundles. Positions of amino acid substitutions in *anillin* mutant alleles are shown below. (C) Sequence alignment near the N terminus of the Anillin PH domain. Sequences from *Drosophila*, human, *Xenopus* and *C. elegans* are shown with a predicted secondary structure below. The amino acid changes for the three strong *scraps* alleles are indicated above. Note that the V to S change at the beginning of the PH domain is present in all Schupbach/Wieschaus alleles sequenced (red arrowhead). (D) Western blot analysis of maternal effect alleles. Embryo extracts from wild-type and three different maternal allelic combinations were probed with antibodies to Anillin and Actin.

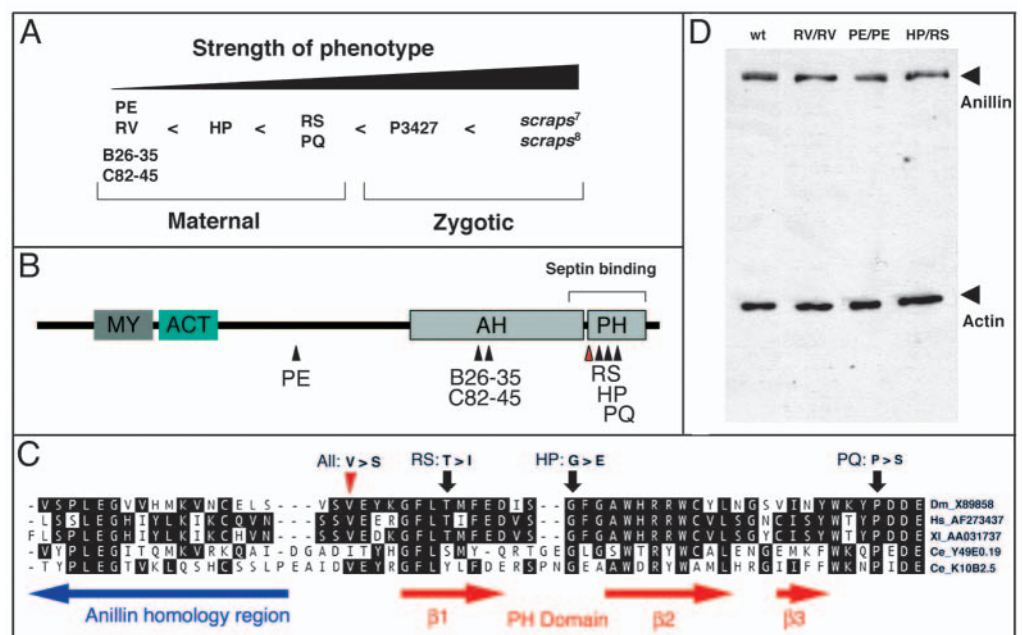
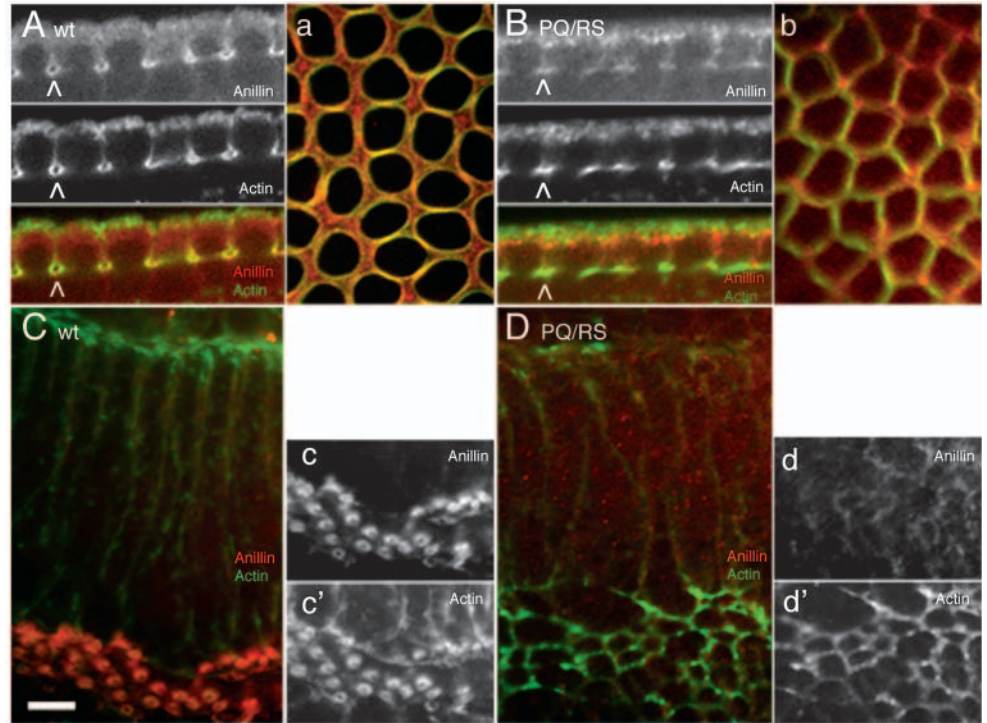


Fig. 2. Anillin and F-actin localization during cellularization. Indirect immunofluorescence of formaldehyde-fixed embryos using laser confocal imaging. (A,C) Wild-type, (B,D) *anillin*^{PQ/RS}-derived embryos. Scale bar: 5 μ m. (A) Wild-type embryo in slow phase, sectioned perpendicular to embryo surface. The teardrop-shaped furrow canals (white arrowheads) contain high levels of Anillin and F-actin. (a) Same embryo, sectioned parallel to the surface at the cellularization front. There is an almost hexagonal network of furrow canals, with Anillin and F-actin partially colocalized in bar-like structures. (B) *anillin*^{PQ/RS}-derived embryo in slow phase, sectioned perpendicular to embryo surface. Furrow canals are malformed (white arrowhead), with lower Anillin levels than wild type. (b) Same embryo, sectioned parallel to the surface at the cellularization front. The network of furrow canals is malformed and partially disorganized, appearing fuzzy. (C) Wild-type embryo in late cellularization/early gastrulation, sectioned perpendicular to embryo surface. Ring-shaped Anillin and F-actin assemblies exist at the base of the newly formed cells (c,c'). The rings sit on top of stalks that connect the cells to the yolk mass (see Fig. S1 in the supplementary material). (D) *anillin*^{PQ/RS}-derived embryo in late cellularization/early gastrulation, sectioned perpendicular to embryo surface. The ring-shaped Anillin and F-actin assemblies are missing (d,d'), and a disorganized F-actin network containing very little Anillin is present at the base of the cells.



substitutions compromise Anillin function, but not its expression or stability.

***anillin* mutations cause defects in contractile ring formation and cellularization fails to complete**

To characterize the role of Anillin in cellularization, we examined the localization of Anillin and three Anillin-interacting proteins (F-actin, Myosin II and septins) in furrow canals of wild-type and *anillin* mutant embryos. Embryos from mothers of four different genotypes (*anillin*^{PQ/RS}, *anillin*^{HP/RS}, *anillin*^{PE/PE}, *anillin*^{RV/RV}) were analyzed. To reduce the possibility of second-site recessive mutations contributing to the phenotype, most of the analysis was performed in embryos derived from *anillin*^{PQ/RS} and *anillin*^{HP/RS} mothers, trans-heterozygotes of strong maternal alleles. That said, similar phenotypes were observed in other allele combinations.

When cellularization begins in nuclear cycle 14, F-actin is enriched in cortical 'caps' that form above each of the nuclei, while Anillin localizes to the region between and around the base of the F-actin caps, where furrow canals will subsequently assemble. Anillin in 'intercap' regions forms a hexagonal network in a plane parallel to the embryo surface (Field and Alberts, 1995). In all *anillin*-derived embryos examined, F-actin and Anillin localized correctly to their respective cortical domains at this early stage (not shown).

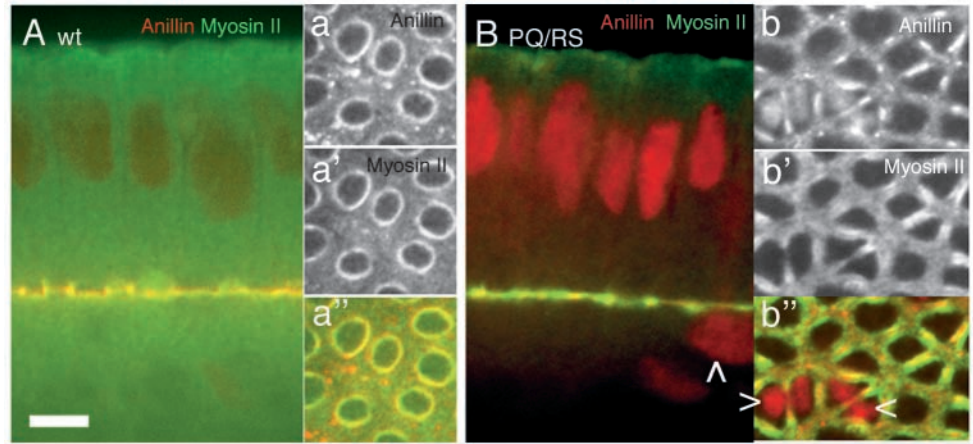
The first significant defects observed were in cellularization. In wild-type embryos, early furrow canals are enriched in Anillin and F-actin (Fig. 2A, arrowheads). In late cellularization/gastrulation, the contractile rings at the base of the newly formed cells are strongly enriched in Anillin which

is colocalized with F-actin (Fig. 2C,c,c'). The contractile rings sit on top of membranous stalks connecting the newly formed cell to the yolk mass (see Fig. S1 in the supplementary material). In embryos from *anillin*^{PQ/RS} mothers, early furrow canals lacked the characteristic 'tear-drop' shape, and the level of Anillin was reduced (Fig. 2B, arrowhead). As these embryos progressed through cellularization, Anillin staining at the cellularization front was further reduced, and the contractile rings failed to form. When gastrulation initiated, little Anillin remained at the cellularization front (Fig. 2D,d) and F-actin staining revealed a broken, hexagonal mesh in place of the normal lattice of rings (Fig. 2D,d'). In summary, in *anillin*^{PQ/RS}-derived embryos there is a progressive loss of Anillin from ingressing furrow canals and the transition from hexagonal network into contractile rings fails. The newly formed cells are open at their bases.

Myosin II localization is disrupted at the cellularization front and cortical nuclei are disorganized

We next probed the effect of *anillin* maternal effect mutations on targeting of Myosin II during cellularization. Early, during slow phase, Myosin II, like Anillin, is strongly enriched in wild-type furrow canals; however, the two signals are not perfectly co-incident and our *anillin* alleles did not exhibit much effect on Myosin II localization (not shown). Later, when contractile rings form (fast phase), Myosin II and Anillin precisely colocalize in the contracting rings (Fig. 3a,a',a''). In *anillin*^{PQ/RS}-derived embryos, where contractile rings fail to form, the Myosin II localization was reduced at the

Fig. 3. Anillin and Myosin II localization during late cellularization. Indirect immunofluorescence of heat, followed by methanol, fixed embryos using laser confocal imaging. (A) Wild type; (B) *anillin*^{PQ/RS}-derived embryos. Scale bar: 5 μ m. (A) Wild-type embryo in late cellularization, sectioned perpendicular to embryo surface. The cellularization front is rich in colocalized Anillin and myosin II. Little Anillin is present in nuclei. (a-a'') Same embryo, sectioned parallel to the surface at the cellularization front. Contractile rings beneath each nucleus are rich in colocalized Anillin and Myosin II. (B) *anillin*^{PQ/RS}-derived embryo in late cellularization, sectioned perpendicular to embryo surface. The cellularization front contains less Anillin. Much of the Anillin has moved into nuclei. Some of the nuclei are mis-positioned (white arrowhead). (b-b'') Same embryo, sectioned parallel to the surface at the cellularization front. Contractile rings are absent. Instead, Anillin and part of the Myosin II are present in abnormal bars. Some nuclei are visible in this plane of section (arrowheads), indicating mis-positioning relative to the embryo surface.



cellularization front (Fig. 3b,b',b''). Myosin II colocalized with mutant Anillin in bar-shaped structures within the disorganized F-actin network (Fig. 3b,b',b''). A similar disruption of Myosin II localization was previously observed in *scraps/anillin* mutants (Thomas and Wieschaus, 2004).

The fixation we used to localize Myosin II (cold methanol) allows for superior observation of mutant Anillin. We observed that when mutant Anillin fails to target normally to the cellularization front, it instead accumulates prematurely in nuclei (compare Fig. 3A,B). In strong alleles, nuclei are commonly disorganized and can become detached from the apical cortex (Fig. 3B,b'', white arrowheads) and we observed excess nuclei in the embryo interior, particularly at the posterior pole (not shown). Anillin is a nuclear protein in interphase tissue culture cells, but in syncytial embryos is normally at the cell cortex until the end of cellularization. The premature nuclear localization we observe in *anillin*^{PQ/RS}-derived embryos suggests that cortical targeting normally competes with nuclear accumulation, and the maternal effect mutations selectively compromise cortical targeting. Abnormal nuclear accumulation of Anillin during cellularization was also observed in syntaxin mutants, another situation where normal furrow canals fail to form (Burgess et al., 1997).

Anillin is required for Peanut localization at the cellularization front

Septin localization was more strongly perturbed by *anillin* mutations. We used antibodies to Peanut, a component of a three-septin complex in embryos (Adam et al., 2000; Fares et al., 1995; Field et al., 1996). Peanut is present and precisely colocalized with Anillin at the cellularization front throughout the entire cellularization process in wild-type embryos (Fig. 4A,C). Peanut alone also localizes to the new plasma membranes between nuclei (Fig. 4C, arrowhead). In embryos derived from *anillin*^{PQ/RS} (Fig. 4B,D) and *anillin*^{HP/RS} (not shown) Peanut localization is strongly perturbed. It fails to colocalize with mutant Anillin in the cellularization front, and it deposits into abnormal puncta at the apical cortex (Fig. 4B,

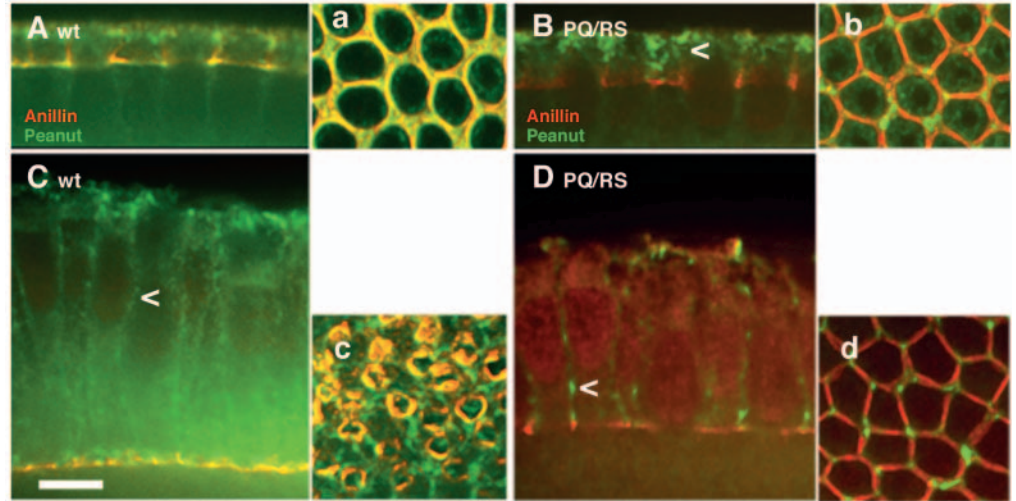
arrowhead) and the plasma membrane (Fig. 4D, arrowhead). By contrast, in embryos derived from weak maternal alleles (*anillin*^{PE/PE} and *anillin*^{RV/RV}) or from weak maternal alleles over a zygotic allele (*anillin*^{B26-35} and *anillin*^{C82-45}/*lanillin*⁸), Peanut localization was normal during slow phase, and the evolution to rings occurred normally in fast phase. However, the rings were less robust and defects in the meshwork were observed (see Fig. S2 in the supplementary material). Because strong *anillin* alleles perturbed the localization of septins to a greater extent than that of F-actin, Myosin II or even Anillin itself, we conclude that these *anillin* mutations, which alter the PH domain, interfere directly with the targeting of septins to their correct cell locations.

Anillin is required for furrow canals to ingress at normal rates

Despite defects in furrow canal structure and septin targeting, the cellularization front still ingresses in *anillin* mutant embryos. To measure ingression kinetics, we examined wild-type and three different mutant genotypes by DIC time-lapse video microscopy. In wild-type, a pronounced cellularization front was evident (Fig. 5A, black arrows). This front was less distinct in all mutant genotypes examined, though its ingression could still be tracked in time-lapse sequences (Fig. 5B, black arrows). Ingression kinetics were measured using kymographs, a method that converts a movie of furrow canal ingression into a graph, with cellularization front depth on the y-axis and time on the x-axis. This method is more sensitive and accurate than tracking the front manually, especially in mutant embryos where it is indistinct in still images. In wild-type embryos (Fig. 5C,D), kymography revealed three stages of ingression identified by two inflection points (white arrows). Each stage lasted ~22 minutes. The first corresponds to organization of furrow canals with little ingression ('initiation phase'). The second and third correspond to slow and fast phases defined previously. The transition between slow and fast phases occurred ~10 μ m from the embryo surface. This analysis is similar to that of Lecuit et al. (Lecuit et al., 2000) with our initiation phase approximately corresponding to their

Fig. 4. Anillin and Peanut (septin) localization during cellularization. Indirect immunofluorescence of cold methanol fixed embryos using laser confocal imaging. (A,C) Wild-type; (B,D) *anillin*^{PQ/RS}-derived embryos. Scale bar: 5 μ m.

(A) Wild-type embryo in slow phase, sectioned perpendicular to embryo surface. The cellularization front is enriched in Anillin and Peanut. (a) Same embryo, sectioned parallel to the surface at the cellularization front, where Anillin and Peanut are almost colocalized. (B) *anillin*^{PQ/RS}-derived embryo in slow phase, sectioned perpendicular to embryo surface. Although Anillin is still present at the cellularization front, Peanut is largely absent, instead it localizes to foci at the apical surface and throughout the cell (arrowhead). (b) Same embryo, sectioned parallel to the surface at the cellularization front. Most of the Peanut is missing, and the remaining protein is present in foci that do not colocalize with Anillin. (C) Wild type embryo in late cellularization/early gastrulation, sectioned perpendicular to embryo surface. Anillin and Peanut colocalize at the cellularization front. The apical and lateral plasma membrane contains Peanut but not Anillin (arrowhead). (c) Same embryo, sectioned parallel to the surface at the cellularization front. Anillin and Peanut colocalize in the rings. (D) *anillin*^{PQ/RS}-derived embryo in late cellularization/early gastrulation, sectioned perpendicular to embryo surface. The cellularization front is disorganized, with most of the Anillin and Peanut missing. Within cells, Peanut is present in abnormal foci (white arrowhead) and nuclei are mis-positioned. (d) Same embryo, sectioned parallel to the surface at the cellularization front. Anillin and Peanut do not colocalize and contractile rings fail to form.



phases 1 and 2, our slow phase to their phase 3, and our fast phase to their phase 4.

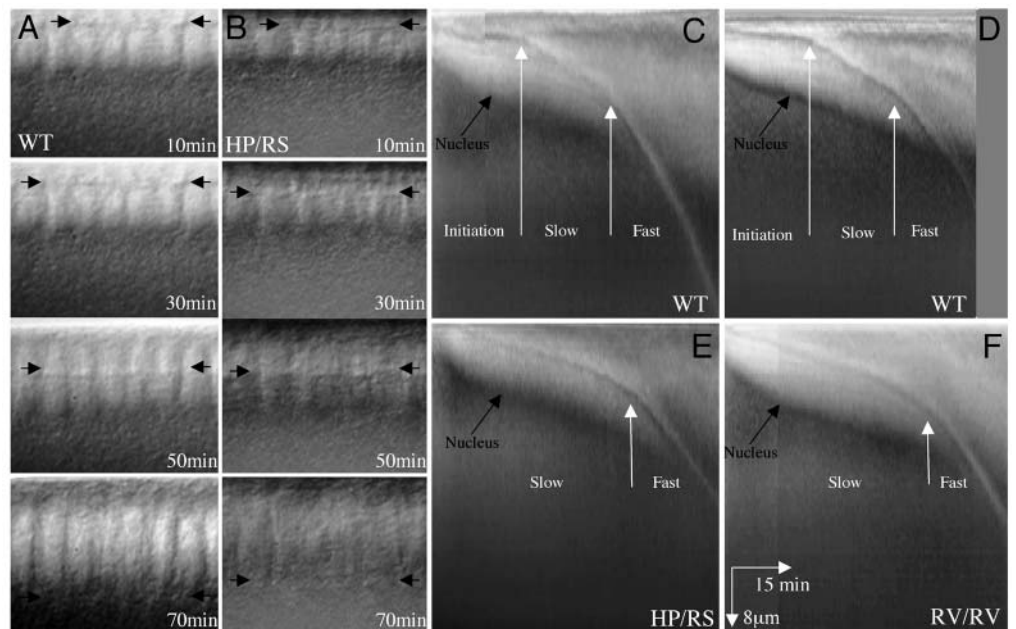
In all three *anillin* mutant genotypes examined, including weak alleles, initiation phase was eliminated. Instead, a

cellularization front began to ingress as soon as mitosis completed, at a rate slower than wild-type slow phase. When the slower-moving front reached a depth similar to the wild-type transition point ($\sim 10 \mu$ m), the rate of ingress increased,

Fig. 5. Time-lapse DIC analysis of cellularization front ingress.

Embryo genotype as indicated. The top of each panel is the embryo surface. (A) In wild-type embryos, a distinct cellularization front (between arrows) can be seen passing through the nuclei. The entire cellularization process takes ~ 70 minutes at 22°C and the membrane ingresses $\sim 35 \mu$ m from the embryo surface. (B) In mutant embryos, the cellularization front (between arrows) is less distinct. (C) Kymograph analysis of a wild-type embryo. A strip perpendicular to the embryo surface, the width of a nucleus, was cut out of time-lapse images as in A. Strips from each frame were pasted together to give a distance versus time plot (scale bars in F). The most obvious line in the kymograph, indicated by the white arrows, is the

cellularization front. Its rate of movement is given by its angle: horizontal indicates static; vertical indicates fast moving. Ingression of the front occurs at three distinct rates, with breaks between them indicated by the white arrows. The black arrow indicates the base of the nucleus, that moves downwards as the nuclei elongate. (D) Second example of a kymograph of a wild-type embryo. (E) Kymograph of an *anillin*^{HP/RS}-derived embryo (strong maternal alleles). No initiation phase is evident. As soon as the front can be tracked, it ingresses at a roughly constant and slow rate. A distinct transition to a faster rate can be observed (white arrow), but both slow and fast rates of ingress are slower than their wild-type counterparts. The black arrow indicates the base of the nucleus, which moves downwards as the nuclei elongate. (F) Kymograph of an *anillin*^{RV/RV}-derived embryo (weak maternal allele). Ingression kinetics are similar to those in E.



but was slower than fast phase in wild-type. We conclude that Anillin normally acts to prevent premature furrow ingression, and that mutant alleles slow the rate of furrow ingression during both slow and fast phases.

Anillin is required for stability of new plasma membranes formed during cellularization

We were puzzled by the disorganization of nuclei at the cortex of *anillin*-derived embryos (Fig. 3B). In many cell-types, nuclear position is dependent on microtubules as well as the F-actin cortex (Reinsch and Gonczy, 1998). We examined the microtubule distribution in *anillin*-derived embryos, but it appeared similar to wild type (not shown). We next examined the newly formed plasma membranes during cellularization, by transmission electron microscopy (TEM) of thin sections of embryos from wild-type and three different mutant genotypes. EM images of wild-type embryos at all stages were similar to those previously published (Fullilove and Jacobson, 1971; Rickoll, 1976; Turner and Mahowald, 1976). Furrow canals were well formed and two closely apposed plasma membranes extended from furrow canal tops to the apical surface of the embryo (Fig. 6A-C). By TEM, *anillin*^{HP/RS}-derived embryos (strong allelic combination) were indistinguishable from wild type in initiation and early slow phase (not shown). However, as the cellularization front ingressed, extensive abnormalities became apparent. Furrow canals were malformed, appearing narrow or absent (Fig. 6D,E), consistent with our confocal fluorescence images. In place of paired plasma membranes between nuclei, we frequently observed lines of small vesicles extending toward the apical

surface (Fig. 6E,F, arrows; Fig. 6H,I). Transformation of apposed plasma membranes into a line of vesicles appeared to be time dependent. Embryos fixed in slow phase showed both paired plasma membranes and lines of vesicles in different areas of the same specimen, while those fixed in fast phase showed only lines of vesicles (Fig. 6H,I). By examining different regions of a single slow phase embryo at high magnification (Fig. 7B-D), we collected images that we interpret as successive stages in a transformation from paired new plasma membranes to vesicles, going through intermediates with convoluted, but still intact, double membrane.

The degree of furrow canal and membrane defects observed by TEM directly corresponds to allelic strength. Embryos derived from *anillin*^{HP/RS} (strong alleles, $n=5$) had the strongest phenotype while those derived from *anillin*^{PE/PE} mothers ($n=6$) had more normal furrow canals and more continuous lateral plasma membranes in later stages of ingression. When the lateral membrane vesiculated in this homozygous weak allele, vesicles were fewer and smaller (not shown and Fig. 8). Embryos derived from *anillin*^{RV/RV} mothers ($n=9$ total, $n=1$ late) looked similar to wild type (not shown).

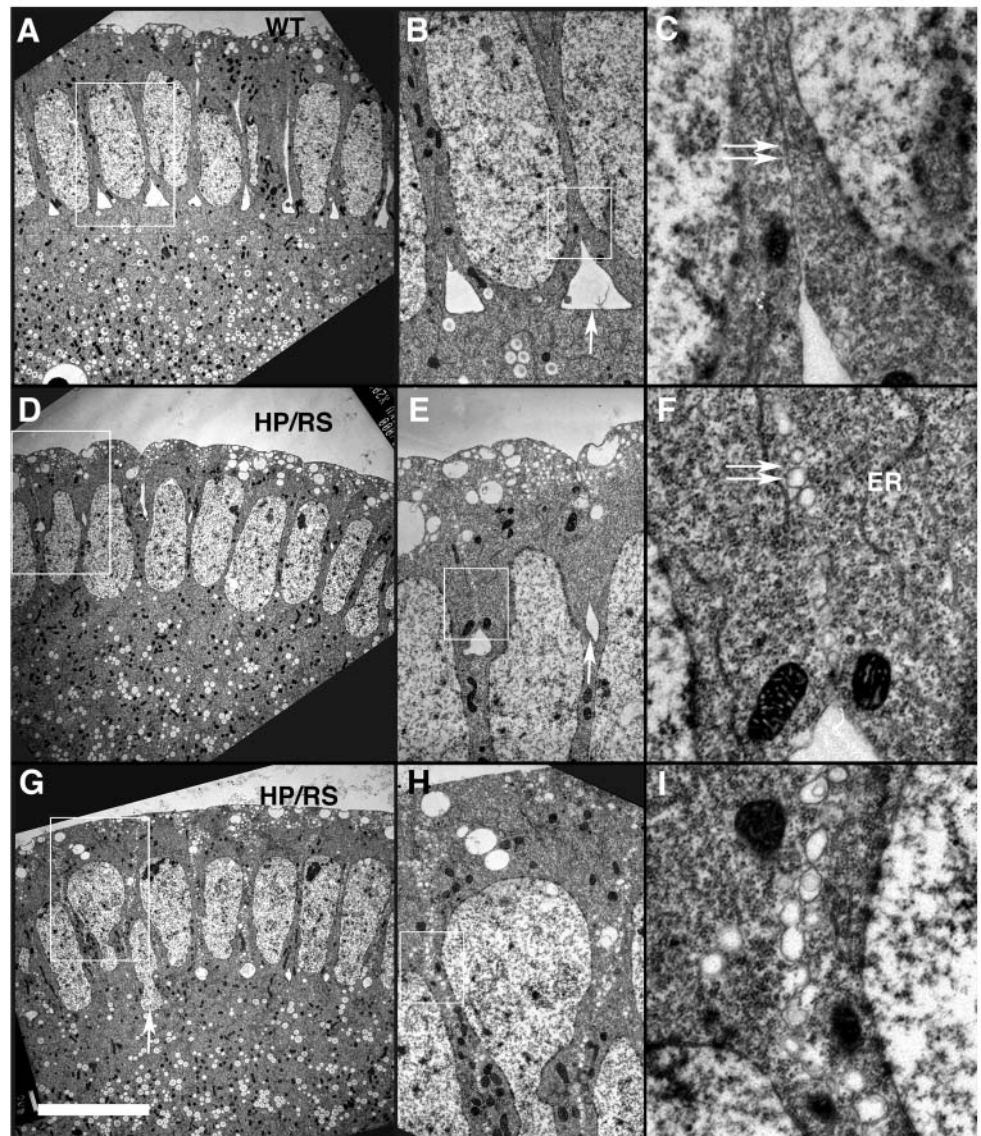


Fig. 6. Thin section transmission electron microscopy (TEM) analysis of cellularization. The boxed areas are presented at higher magnification in the panels on the right. (A-C) Wild-type embryo, fast phase. Note the almost triangular furrow canals (arrow in B) and the almost straight, closely apposed plasma membranes that connect the top of the furrow canal to the embryo surface (double arrow in C). (D-F) *anillin*^{HP/RS}-derived embryo, slow phase. Furrow canals are lacking (D) or malformed (arrow in E). There are no paired plasma membranes at the top of the furrow canal in F. A line of vesicles is present in its place (double arrows). ER in F indicates an ER lamella. (G-I) *anillin*^{HP/RS}-derived embryo in fast phase. The nucleus is mis-positioned (arrow in G). All plasma membranes between nuclei are vesiculated at this stage. Scale bar: 10 μm in A,D,G; 4 μm in B,E,H; 0.8 μm in C,F,I.

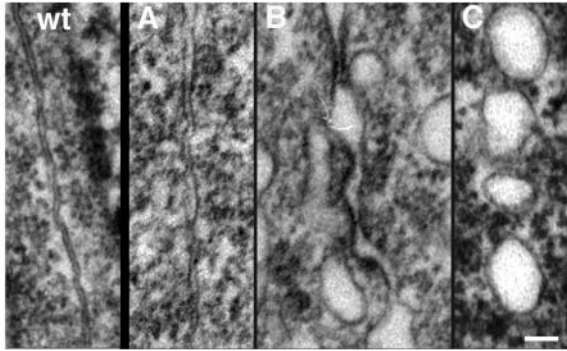


Fig. 7. High magnification TEM of new plasma membranes. Left-hand panel shows a wild-type embryo. The paired plasma membranes are fairly straight, and a constant distance apart. (A–C) *anillin*^{HP/RS}-derived, slow phase embryo (the same embryo shown in Fig. 6D–F). The panels show different positions in the same embryo, all between furrow canals and the surface. (A) The paired plasma membranes are almost normal, though the distance between them is variable. (B) The membranes are still almost continuous, but they are highly distorted and electron-dense material is present on the membrane. (C) The membrane is completely vesiculated, similar to the region shown in Fig. 6F. Scale bar: 150 nm.

Vesiculation of membranes can be induced as an artifact of poor fixation, presenting a possible problem in interpreting our EM images. Arguing against this, vesiculation of apposed plasma membranes was never observed in wild-type embryos ($n=9$) and always in embryos derived from *anillin*^{HP/RS} mothers. Vesiculation was also specific for the new, apposed plasma membranes. It was not observed for plasma membrane at the embryo surface, in furrow canals, or around pole cells (see below), nor for endoplasmic reticulum membranes (Fig. 6F, ER), even when these were adjacent to vesiculated plasma membranes (Fig. 6F, double arrows). To confirm plasma membrane defects at the light level, we imaged Neurotactin, a trans-membrane protein that is inserted continuously into the new plasma membranes during slow and fast phases (Lecuit and Wieschaus, 2000). By confocal immunofluorescence, Neurotactin localized to a smooth, straight line at the apposed plasma membrane of cellularizing wild-type embryos, and to a fuzzy, irregular line in strong maternal effect *anillin* alleles (see Fig. S3 in the supplementary material). Although we cannot rule out fixation-induced vesiculation, these data imply that Anillin function is required specifically for stability of the new, apposed, lateral plasma membranes.

Anillin is required for pole cell formation

TEM also revealed effects of *anillin* mutations on pole cell separation, a specialized type of cytokinesis that defines the presumptive germ cells (Foe et al., 1993). Analysis by TEM indicated that wild-type embryos late in cycle 14 possess well-separated, almost spherical pole cells, containing characteristically round nuclei at their posterior pole. Pole cells occupy a layer outside the cellularizing blastoderm and are also interspersed between incipient blastoderm cells (Fig. 8A). In *anillin*^{HP/RS}-derived embryos (a strong allele combination), pole cells were properly formed and were enclosed by intact spherical plasma membranes as in wild type (Fig. 8B,b). This normal morphology was remarkable given the abnormally

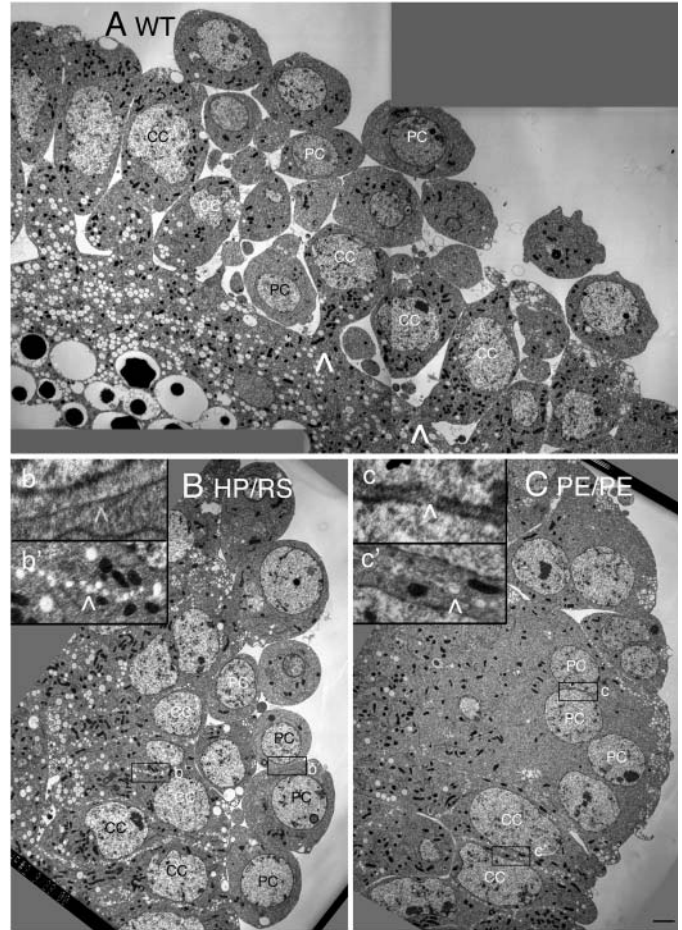
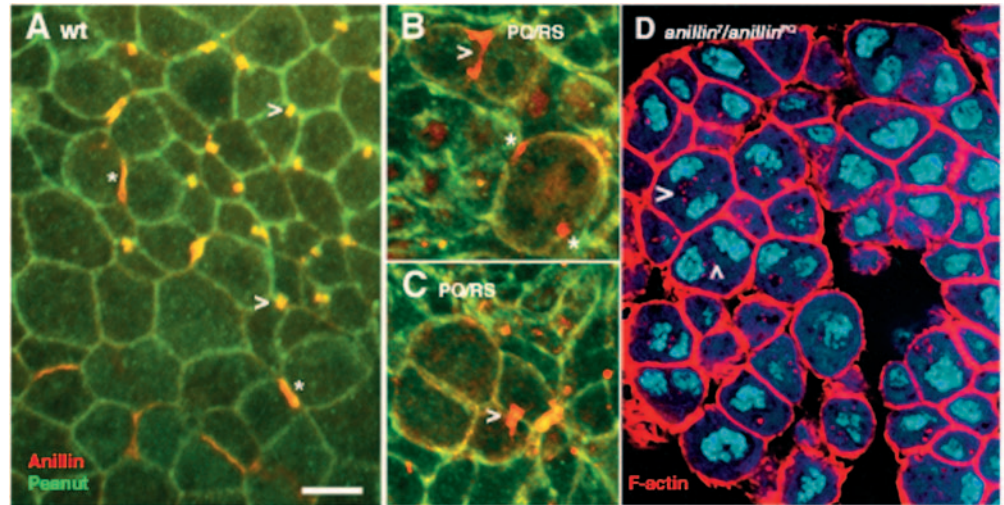


Fig. 8. TEM analysis of pole cells. Wild-type embryo in fast phase, showing a region near the posterior end of the embryo. PC, pole cell nucleus with characteristic round morphology with smooth nuclear envelope. CC, cellularizing cell nucleus. Stalks connecting the cells to the yolk mass (white arrows). (A) *anillin*^{HP/RS}-derived embryo, late cellularization/early gastrulation. Cellularization is failing, but pole cell separation is almost normal. Boxed areas are shown at higher magnification in the insets. (B,b') Paired plasma membranes between two pole cells appear normal. (B,b'') Paired plasma membranes between two cellularized cells have completely vesiculated. *anillin*^{PE/PE} derived embryo, late cellularization/early gastrulation. Cellularization is less perturbed than (C) in this weaker allele, but pole cell separation has failed completely. Boxed areas are shown at higher magnification in the insets. (c) No plasma membrane or vesicles are present between pole cell nuclei. (c') Partially vesiculated plasma membranes are present between the nuclei of cellularized cells. Scale bar: 2 μ m in main panels, 0.5 μ m in insets.

positioned nuclei and vesiculated lateral plasma membranes (Fig. 8b') of incipient blastoderm cells in the same embryo. By contrast, *anillin*^{PE/PE}-derived embryos completely lacked separated pole cells by TEM. Numerous pole cell nuclei were present at the posterior pole, but no plasma membranes separated them from the rest of the blastoderm (Fig. 8C) and no membranes were observed between nuclei (Fig. 8c). In keeping with the weaker allele strength, there is less vesiculation of the lateral membrane in this genotype (Fig. 8c').

The presence of pole cell nuclei with normal morphology and number suggest that the mutation perturbs separation,

Fig. 9. Immunofluorescence analysis of conventional cytokinesis. (A) Mitotic domain, wild-type embryo. Anillin and Peanut colocalize in cleavage furrows (*) and intracellular bridges (arrowheads). Intracellular bridges are long lasting, and were frequently observed in mitotic domains. (B) Mitotic domain, *anillin*^{PQ/RS}-derived embryo. Mutant Anillin, but not Peanut, is localized to cleavage furrows (arrowhead) and to an apparently regressed cleavage furrow in a bi-nucleate cell (*). (C) Genotype as in B. Example of a rare intracellular bridge enriched in Anillin but not septins (arrowhead). Intracellular bridges were very rare, indicating that most attempts at cytokinesis fail. (D) Imaginal disc rudiment from 3rd instar larvae, genotype *anillin*⁷/*anillin*^{PQ} stained for F-actin (red) and DNA (blue). Large binucleate cells (arrowheads) are present. Scale bar: 5 μ m.



rather than specification, of pole cells. Time-lapse DIC analysis showed that embryos from *anillin*^{PE/PE} mothers formed pole cells transiently, but that the furrows separating them from the rest of the embryo regressed at the end of each nuclear cycle (data not shown). This furrow regression phenotype was not seen in the three other genotypes examined, including two heterozygotes of strong alleles. The *anillin*^{PE/PE} lesion maps to an unexplored region of Anillin that has not been implicated in septin interactions (Fig. 1B).

Anillin is required maternally and zygotically for conventional cytokinesis

To determine whether Anillin is required for conventional cytokinesis in embryos, we imaged contractile rings in mitotic domains following cellularization. Embryos were fixed and co-stained for F-actin (not shown), Anillin and Peanut. In the mitotic domains of wild-type embryos (Fig. 9A), Anillin and Peanut colocalize in cleavage furrows (asterisks) and intracellular bridges (arrowheads). Although cleavage furrows formed and contracted in embryos derived from *anillin*^{PQ/RS} mothers, they appeared to regress (Fig. 9B, asterisks), and very few intracellular bridges were observed, except for rare aberrant structures (Fig. 9C, arrowhead). Anillin recruitment to cleavage furrows was not perturbed, and may even have increased. Peanut failed to concentrate in cytokinesis furrows (Fig. 9B, white arrowhead and asterisks). F-actin was present at wild-type amounts (not shown).

To test for a zygotic requirement for Anillin in cytokinesis, we examined cells in imaginal discs isolated from mutant 3rd instar larvae (genotype *anillin*⁷/*anillin*^{PQ}) probing for F-actin and DNA. Embryos of this genotype survive to pupation but die before eclosion. All discs dissected were much smaller than wild type and difficult to identify. The rudimentary discs contained many large bi-nucleate cells (Fig. 9D), implying failure of cytokinesis. We conclude Anillin is required for normal cytokinesis in *Drosophila* embryos, and that strong maternal alleles block recruitment of Peanut (but not of Anillin or Actin) to cleavage furrows.

Discussion

Anillin-septin interactions

The strongest molecular conclusion from our work is that Anillin is required to target and maintain septins in cortical structures. Strong maternal *anillin* alleles map to the N terminus of the PH domain, the region of Anillin previously predicted to interact with septins on the basis of fragment expression (Oegema et al., 2000) and in vitro binding assays (Kinoshita et al., 2002). These alleles cause severe mis-localization of the septin Peanut and also result in a significant reduction in the amount of Anillin in furrow canals late in cellularization. Thus, the genetic and biochemical data together suggest that a physical interaction between the PH domain of Anillin and septin complexes is required to stably recruit both proteins to ingressing furrow canals. This interdependence is also supported by analysis of Peanut mutants (Adam et al., 2000). In embryos that lack Peanut, F-actin rings failed to form late in cellularization, similar to strong *anillin* alleles. Anillin localization was normal in slow phase, but the protein was progressively lost from furrow canals during fast phase, showing that Peanut is necessary for stable localization of Anillin. A role for Anillin in targeting and stabilizing septins is also supported by studies in *C. elegans*, where the Anillin homolog ANI-1 is required to target the septins to the contractile ring (Maddox et al., 2005), and in *S. pombe*, where the Anillin-related protein Mid2 stabilizes cortical septins in the medial ring (Berlin et al., 2003; Tasto et al., 2003).

PH domains in many proteins have been implicated in lipid binding, and the amino acid changes in our strong *anillin* alleles fall in the region of this domain known to interact with lipids (Lemmon, 2004; Rameh et al., 1997). However, the PH domain of Anillin lacks the positively charged amino acids that mediate specific binding to phosphoinositides, and GFP fusions to the C terminus of human Anillin transiently expressed in mammalian cells did not localize to the plasma membrane, but instead assembled into small septin-containing foci (Oegema et al., 2000). It therefore seems possible that the PH domain of Anillin mediates a protein-protein interaction with septins and

not a protein-lipid interaction. However, *Drosophila* Anillin can target to the cellularization front in the absence of Peanut (Adam et al., 2000) and the *C. elegans* ortholog ANI-1 can target to the furrow normally in the absence of the septins (Maddox et al., 2005). Many PH domains do not bind inositol lipids with high affinity and require oligomerization or additional motifs within the same protein to impart membrane localization (Lemmon et al., 2002). It is therefore possible that the PH domain of Anillin mediates association with membranes by mechanisms other than septin binding.

The role of Anillin in membrane stabilization

Morphologically, the most dramatic phenotype of strong *anillin* alleles was the appearance of sheets of vesicles (that appear as lines in thin sections) between nuclei during cellularization, in place of the intact, apposed plasma membranes deposited behind the cellularization front in wild-type embryos. We interpret the presence of some intact membranes in mutant embryos fixed early in cellularization (Fig. 7), as evidence that lateral plasma membranes are initially deposited in *anillin* mutant embryos, but they are unstable and subsequently vesiculate. Other membranes in the mutant embryos, including pole cell and apical plasma membranes, are unaffected, arguing that vesiculation is not a fixation artifact, and that the new lateral plasma membranes have a specific requirement for Anillin and septins for stability. These membranes are special in at least three ways that might account for their fragility: they assemble very rapidly, by highly dynamic exo- and endocytosis (Lecuit and Wieschaus, 2000; Pelissier et al., 2003); they are probably under tension from the ingressing furrow canals; and they are closely apposed to each other. Anillin might regulate vesicle trafficking dynamics; for example, decreasing exocytosis could lead to a build up of tension and membrane fragmentation. Septins have been argued to regulate exocytosis in mammalian cells but, in this case, inactivation of septins leads to increased, rather than decreased, exocytosis (Beites et al., 1999). Alternatively, Anillin might directly regulate physical stability of membranes. Plasma membranes are physically stabilized in most situations by attachment to a cortical actin cytoskeleton, and loss of Anillin might destabilize them by weakening the cortex or its attachment to the membrane. Destabilization of membranes under tension might lead to the fusion of closely apposed membranes and the lines of vesicles we observe are reminiscent of some stages of programmed cell fusion, e.g. myoblast fusion (Doberstein et al., 1997). Anillin itself does not localize to the cortex of the apposed plasma membranes, but it might function to recruit and leave behind other proteins required for stability under tension. Septins are normally present and localized ectopically in *anillin* mutants; although targeting of F-actin is less affected, its organization in mutants is unknown. Loss of septins or F-actin bundling could result in a more fragile, or more weakly attached, cortical cytoskeleton, causing the membranes to fragment as tension builds up during cellularization. A role for septins in stabilizing membranes could be tested by TEM of *peanut* mutant embryos, which are known to exhibit defects in nuclear positioning similar to those we observe in *anillin* mutants (Adam et al., 2000). Roles for Anillin in regulating membrane trafficking compared with physical stability might be distinguished by live imaging of membrane markers to measure exo- and endocytosis, and by

imaging thermal fluctuations of the new plasma membranes to estimate their stiffness, as a function of *anillin* genotype.

An interesting aspect of the vesiculation phenotype is the tendency of plasma membrane-derived vesicles to remain localized in sheets behind the cellularization front, rather than diffusing away. We suspect they may be adhering to the baskets of microtubules that surround each nucleus (Foe et al., 1993), that were unaffected in *anillin* mutant embryos. Remarkably, the physical organization of vesicles is sufficient to allow gastrulation movements (not shown), even though cellularization has failed completely in terms of generating cells bounded by plasma membranes.

A role for Anillin in organizing contractile structures

Although defects in septin recruitment mirrored our allelic series, septin recruitment is clearly not the only function of Anillin. We observed similar defects in the timing and rate of cellularization front ingression in all alleles examined, including weak alleles that had no obvious defects in septin recruitment. We also observed defects in F-actin and Myosin II localization/organization that are consistent with previously identified biochemical interactions (Field and Alberts, 1995; Straight et al., 2005). As our alleles did not alter the N terminus of Anillin, where it interacts with F-actin and Myosin II, these defects probably result from reduced localization of functional Anillin. A role for Anillin in scaffolding contractile structures has been demonstrated in *C. elegans*, where the Anillin homolog ANI-1 is required to organize foci containing Myosin II that pull on the plasma membrane during polarity establishment (Maddox et al., 2005). Focusing of actomyosin contraction by Anillin is also suggested by excessive membrane blebbing and mislocalization of myosin II seen during cytokinesis after knocking down Anillin by RNAi (Echard et al., 2004; Somma et al., 2002; Straight et al., 2005).

A more structural role for Anillin may be important late in cytokinesis and cellularization. Myosin II, and most F-actin, typically leave furrows before cytokinesis is complete, and it is important that something prevents the furrow from opening back up when it is no longer actively contractile. Anillin and septins may assemble into a structure under the plasma membrane to stabilize the neck of cytoplasm late in cytokinesis. One allele, *anillin*^{PE/PE}, exhibited a severe effect on pole cell formation because of re-opening of the neck of cytoplasm connecting the pole cell to the yolk mass. Interestingly, this allele exhibited milder defects in cellularization, was viable over zygotic mutations and thus was termed 'weak'. The mutation maps to a region in the middle of Anillin not implicated in any protein interactions. In other systems, removal of Anillin also leads to defects late in cytokinesis, with furrows reopening (Echard et al., 2004; Somma et al., 2002; Rogers et al., 2003; Straight et al., 2005). Anillin and septins are strongly enriched as rings or short tubes in stable intracellular bridges, including male ring canals during spermatogenesis (Hime et al., 1996; Robinson and Cooley, 1996), and the stalks that connect cells to the yolk mass after cellularization (see Fig. S1 in the supplementary material, Fig. 2 and Fig. 4). They also remain in mid-bodies after the contractile proteins leave during conventional cytokinesis (Field and Alberts, 1995). Cumulatively, these data suggests that ring- or tube-shaped Anillin-septin assemblies [rings are the preferred assembly state of mammalian septins (Kinoshita et al., 2002)] may stabilize

intracellular bridges to facilitate the completion of normal cytokinesis, and to allow communication between sister cells following incomplete cytokinesis.

Given its interaction with multiple conserved furrow proteins, and its functional involvement in both contractility and membrane stability, further study of Anillin is likely to reveal detailed aspects of how the cytoskeleton and membrane systems work together during cytokinesis, and related furrowing processes in embryos.

We thank Karen Oegema, Amy Maddox, Ulrike Eggert and Tim Mitchison for critical reading of the manuscript; Kristine Yu and Julie Brill for help with the rescue experiment; James Cordero for early efforts on the project and DIC movies pole cell formation in *anillin* alleles. C.M.F. thanks Eric Wieschaus and Trudi Schupach for the original *scraps* alleles, sharing unpublished data and encouragement; Ruth Lehmann for sharing unpublished data; and Jennifer Waters at the HMS/Nikon Imaging Center for help with microscopy. For support and guidance, T.M. thanks Ruth Lehmann, in whose laboratory part of this work was performed. C.M.F. and M.C. are supported by NIH GM23928. T.M. was supported by EMBO and a fellowship of the International Human Frontier Science Program Organization. W.S. is supported by NIH GM 58903.

Supplementary material

Supplementary material for this article is available at <http://dev.biologists.org/cgi/content/full/132/12/2849/DC1>

References

- Adam, J. C., Pringle, J. R. and Peifer, M. (2000). Evidence for functional differentiation among *Drosophila* septins in cytokinesis and cellularization. *Mol. Biol. Cell* **11**, 3123-3135.
- Beites, C. L., Xie, H., Bowser, R. and Trimble, W. S. (1999). The septin CDCrel-1 binds syntaxin and inhibits exocytosis. *Nat. Neurosci.* **5**, 434-439.
- Berlin, A., Paoletti, A. and Chang, F. (2003). Mid2p stabilizes septin rings during cytokinesis in fission yeast. *J. Cell Biol.* **160**, 1083-1092.
- Burgess, R. W., Deitcher, D. L. and Schwarz, T. L. (1997). The synaptic protein syntaxin1 is required for cellularization of *Drosophila* embryos. *J. Cell Biol.* **138**, 861-875.
- Doberstein, S. K., Fetter, R. D., Mehta, A. Y. and Goodman, C. S. (1997). Genetic analysis of myoblast fusion: blown fuse is required for progression beyond the prefusion complex. *J. Cell Biol.* **136**, 1249-1261.
- Edchard, A., Hickson, G. R., Foley, E. and O'Farrell, P. H. (2004). Terminal cytokinesis events uncovered after an RNAi screen. *Curr. Biol.* **14**, 1685-1693.
- Fares, H., Peifer, M. and Pringle, J. R. (1995). Localization and possible functions of *Drosophila* septins. *Mol. Biol. Cell* **6**, 1843-1859.
- Field, C. M. and Alberts, B. M. (1995). Anillin, a contractile ring protein that cycles from the nucleus to the cell cortex. *J. Cell Biol.* **131**, 165-178.
- Field, C. M. and Kellogg, D. (1999). Septins: cytoskeletal polymers or signalling GTPases? *Trends Cell Biol.* **9**, 387-394.
- Field, C. M., al-Awar, O., Rosenblatt, J., Wong, M. L., Alberts, B. and Mitchison, T. J. (1996). A purified *Drosophila* septin complex forms filaments and exhibits GTPase activity. *J. Cell Biol.* **133**, 605-616.
- Finger, F. P. and White, J. G. (2002). Fusion and fission: Membrane trafficking in animal cytokinesis. *Cell* **108**, 727-730.
- Foe, V. E. (1989). Mitotic domains reveal early commitment of cells in *Drosophila* embryos. *Development* **107**, 1-22.
- Foe, V. E., Odell, G. M. and Edgar, B. A. (1993). Mitosis and morphogenesis in the *Drosophila* embryo: point and counterpoint. In *The Development of Drosophila melanogaster*, Vol. 1 (ed. M. Bate and A. M. Arias), pp. 149-300. Plainview, NY: Cold Spring Harbor Press.
- Foe, V. E., Field, C. M. and Odell, G. M. (2000). Microtubules and mitotic cycle phase modulate spatiotemporal distributions of F-actin and myosin II in *Drosophila* syncytial embryos. *Development* **127**, 1767-1787.
- Fullilove, S. L. and Jacobson, A. G. (1971). Nuclear elongation and cytokinesis in *Drosophila montana*. *Dev. Biol.* **26**, 560-577.
- Heitzler, P., Coulson, D., Saenz-Robles, M., Ashburner, M., Roote, J., Simpson, P. and Gubb, D. (1993). Genetic and cytogenetic analysis of the 43 A-E region containing the segment polarity gene *costa* and the cellular polarity genes *prickle* and *spiny-legs* in *Drosophila melanogaster*. *Genetics* **135**, 105-115.
- Hime, G. R., Brill, J. A. and Fuller, M. T. (1996). Assembly of ring canals in the male germ line from structural components of the contractile ring. *J. Cell Sci.* **109**, 2779-2788.
- Kiger, A. A., Baum, A., Jones, S., Jones, M. R., Coulson, A., Escheverri, C. and Perrimon, N. (2003). A functional genomic analysis of cell morphology using RNAi interference. *J. Biol.* **2**, 1-15.
- Kinoshita, M., Field, C. M., Coughlin, M. L., Straight, A. F. and Mitchison, T. J. (2002). Self- and actin-templated assembly of Mammalian septins. *Dev. Cell* **3**, 791-802.
- Lecuit, T. and Wieschaus, E. (2000). Polarized insertion of new membrane from a cytoplasmic reservoir during cleavage of the *Drosophila* embryo. *J. Cell Biol.* **150**, 849-860.
- Lemmon, M. A. (2004). Pleckstrin homology domains: not just for phosphoinositides. *Biochem. Soc. Trans.* **32**, 707-711.
- Lemmon, M. A., Ferguson, K. M. and Abrams, C. S. (2002). Pleckstrin homology domains and the cytoskeleton. *FEBS Lett.* **513**, 71-76.
- Maddox, A. S., Habermann, B., Desai, A. and Oegema, K. (2005). Distinct roles for two *C. elegans* anillins in the gonad and early embryo. *Development* **132**, 2837-2848.
- Mitchison, T. J. and Field, C. M. (2002). Cytoskeleton: what does GTP do for septins? *Curr. Biol.* **12**, R788-R790.
- O'Halloran, T. J. (2000). Membrane traffic and cytokinesis. *Traffic* **1**, 921-926.
- Oegema, K., Savoian, M. S., Mitchison, T. J. and Field, C. M. (2000). Functional analysis of a human homologue of the *Drosophila* actin binding protein anillin suggests a role in cytokinesis. *J. Cell Biol.* **150**, 539-552.
- Paoletti, A. and Chang, F. (2000). Analysis of mid1p, a protein required for placement of the cell division site reveals a link between the nucleus and the cell surface in fission yeast. *Mol. Biol. Cell* **8**, 2751-2773.
- Peifer, M., Sweeton, M., Casey, M. and Wieschaus, E. (1994). Wingless signal and Zeste-white 3 kinase trigger opposing changes in the intracellular distribution of Armadillo. *Development* **120**, 369-380.
- Pelissier, A., Chauvin, J. P. and Lecuit, T. (2003). Trafficking through Rab11 endosome is required for cellularization during *Drosophila* embryogenesis. *Curr. Biol.* **13**, 1848-1857.
- Rameh, L. E., Arvidsson, A., Carraway, K. L., 3rd, Couvillon, A. D., Rathbun, G., Crompton, A., VanRenterghem, B., Czech, M. P., Ravichandran, K. S., Burakoff, S. J. et al. (1997). A comparative analysis of the phosphoinositide binding specificity of pleckstrin homology domains. *J. Biol. Chem.* **272**, 22059-22066.
- Reinsch, S. and Goczny, P. (1998). The mechanisms of nuclear positioning. *J. Cell Sci.* **111**, 2283-2295.
- Rickoll, W. L. (1976). Cytoplasmic continuity between embryonic cells and the primitive yolk sac during early gastrulation in *Drosophila melanogaster*. *Dev. Biol.* **49**, 304-310.
- Robinson, D. N. and Cooley, L. (1996). Stable intercellular bridges in development: the cytoskeleton lining the tunnel. *Trends Cell Biol.* **6**, 474-479.
- Rogers, S. L., Wiedmann, U., Stuurmann, N. and Vale, R. D. (2003). Molecular requirements for actin-based lamella formation in *Drosophila* S2 Cells. *J. Cell Biol.* **162**, 1079-1088.
- Royou, A., Field, C., Sisson, J. C., Sullivan, W. and Karess, R. (2004). Reassessing the role and dynamics of nonmuscle myosin II during furrow formation in early *Drosophila* embryos. *Mol. Biol. Cell* **15**, 838-850.
- Schejter, E. D. and Wieschaus, E. (1993). Functional elements of the cytoskeleton in the early *Drosophila* embryo. *Annu. Rev. Cell Biol.* **9**, 67-99.
- Schupbach, T. and Wieschaus, E. (1989). Female sterile mutations on the second chromosome of *Drosophila melanogaster*. I. Maternal effect mutations. *Genetics* **121**, 101-117.
- Serano, T. L., Cheung, H. K., Frank, L. H. and Cohen, R. S. (1994). P element transformation vectors for studying *Drosophila melanogaster* oogenesis and early embryogenesis. *Gene* **138**, 181-186.
- Somma, M. P., Fasulo, B., Cenci, G., Cundari, E. and Gatti, M. (2002). Molecular dissection of cytokinesis by RNA interference in *Drosophila* cultured cells. *Mol. Biol. Cell* **13**, 2448-2460.
- Straight, A. F., Field, C. M. and Mitchison, T. J. (2005). Anillin binds nonmuscle Myosin II and regulates the contractile ring. *Mol. Biol. Cell* **1**, 193-201.
- Tasto, J. J., Morrell, J. L. and Gould, K. L. (2003). An anillin homologue, Mid2p, acts during fission yeast cytokinesis to organize the septin ring and promote cell separation. *J. Cell Biol.* **160**, 1093-1103.
- Thomas, J. H. and Wieschaus, E. (2004). src64 and tec29 are required for

microfilament contraction during *Drosophila* cellularization. *Development* **131**, 863-871.

Trimble, W. S. (1999). Septins: a highly conserved family of membrane-associated GTPases with functions in cell division and beyond. *J. Membr. Biol.* **169**, 75-81.

Turner, F. R. and Mahowald, A. P. (1976). Scanning electron microscopy of *Drosophila* embryogenesis. 1. The structure of the egg envelopes and the formation of the cellular blastoderm. *Dev. Biol.* **50**, 95-108.

Warn, R. M. and Robert-Nicoud, M. (1990). F-actin organization during the cellularization of the *Drosophila* embryo as revealed with a confocal laser scanning microscope. *J. Cell Sci.* **96**, 35-42.

Young, P. E., Pesacreta, T. C. and Kiehart, D. P. (1991). Dynamic changes in the distribution of cytoplasmic myosin during *Drosophila* embryogenesis. *Development* **111**, 1-14.